The mechanical properties of freestanding electroplated Cu thin films

Y. Xiang
Division of Engineering and Applied Sciences, Harvard University, Cambridge, Massachusetts 02138

T.Y. Tsui
Texas Instruments, Inc., Dallas, Texas 75243

J.J. Vlassak[a)]
Division of Engineering and Applied Sciences, Harvard University, Cambridge, Massachusetts 02138

(Received 30 December 2005; accepted 22 March 2006)

The plane-strain bulge test is used to investigate the mechanical behavior of freestanding electroplated Cu thin films as a function of film thickness and microstructure. The stiffness of the films increases slightly with decreasing film thickness because of changes in the crystallographic texture and the elastic anisotropy of Cu. Experimental stiffness values agree well with values derived from single-crystal elastic constants and the appropriate orientation distribution functions. No modulus deficit is observed. The yield stress of the films varies with film thickness and heat treatment as a result of changes in the grain size of the films. The yield stress follows typical Hall-Petch behavior if twins are counted as distinct grains, indicating that twin boundaries are effective barriers to dislocation motion. The Hall-Petch coefficient is in good agreement with values reported for bulk Cu. Film thickness and crystallographic texture have a negligible effect on the yield stress of the films.

I. INTRODUCTION

Over the last few decades, much work has gone into characterizing the mechanical behavior of thin metal films. It is found that thin-film mechanical properties are typically very different from those of bulk materials.[1,2] For example, thin metal films are often found to support much higher stresses than their bulk counterparts. This strengthening has generally been attributed to dimensional and microstructural constraints on dislocation motion. Dimensional constraints are imposed by interfaces and the small dimensions typically encountered in thin films, whereas microstructural constraints arise from the very fine grains often found in thin films.[3] In bulk materials, microstructural constraints dominate the plastic behavior of the material. However, when material dimensions are comparable with microstructural length scales, as is typically the case for thin films, free surfaces and interfaces are important as well. For example, dislocations can exit the material through free surfaces, and strong interfaces can prevent them from doing so. Consequently, strong interfaces may lead to a higher cumulative dislocation density in the film, resulting in higher flow stresses and greater strain hardening rates. This strengthening behavior scales with film thickness and is often referred to in this article as the film thickness effect. The film thickness effect has been modeled by various researchers. Theoretical models generally fall into two main categories: The macroscopic models are based on the continuum theory of plasticity, such as the strain gradient plasticity theories by Aifantis[4,5] or Fleck and Hutchison.[6–9] The microscopic models are based on dislocation mechanics, such as the single dislocation model proposed by Nix,[2] or the discrete dislocation dynamics simulations by Needleman and van der Giessen.[10,11]

Compared with dimensional constraints, the effects of microstructural constraints have been widely studied in bulk materials, and various models are well established. For example, the Taylor relationship provides a relationship between flow stress and dislocation density, and the well-known Hall-Petch equation quantifies the effect of the grain size.[12] Some of these models developed for bulk materials break down for materials with very fine microstructures. Spaepen and Yu,[13] for instance, recently compared the effect of microstructural length scales on the yield stress of various Cu-based materials including multilayers, thin films, and nanocrystalline compacts. They found that the classical Hall-Petch relation tends to overestimate the strength as the relevant microstructural length scale decreases below 1 μm or so. Furthermore,

[a)]Address all correspondence to this author.
e-mail: vlassak@esag.deas.harvard.edu
DOI: 10.1557/JMR.2006.0195

 © 2006 Materials Research Society

research on nanocrystalline materials reveals that when the grain size decreases below a critical value (on the order of 10 nm), some materials may exhibit an inverse Hall-Petch behavior, where the flow stress decreases with decreasing grain size.[14,15] This behavior has been attributed to grain boundary deformation mechanisms such as grain boundary sliding and rotation that become dominant at very small grain sizes.[16]

In addition to thin-film plastic behavior, elastic properties are of interest as well. Recent measurements of Young's modulus of various freestanding metal films and multilayers, including Cu,[17–20] Ag,[17] Al,[17,19,21] W,[19] Au,[22,23] and Cu/Ag multilayers,[17] have yielded experimental values that are 20%–50% smaller than for bulk materials, and other researchers have reported values similar to those of bulk materials.[22–28] This modulus deficit is observed mainly for films deposited with e-beam evaporation and tested using the microtensile technique,[17,18,21,22] although sputtered Au films with ultra-fine grains[23] and some electroplated Cu films[20] have also been reported to have lower moduli. Several mechanisms have been suggested to explain the modulus deficit, including incomplete cohesion of grain boundaries, the presence of voids or microcracks, and compliant grain boundaries.[17]

Recently, thin-film studies have focused on Cu because of the adoption of Cu metallization in advanced integrated circuits. Flinn[29] and Thouless et al.[30] investigated stress development and relaxation in Cu films during thermal cycling using the substrate curvature technique. Keller et al.[31] quantitatively studied the effects of film thickness, grain size, and passivation on the yield stress of sputtered thin Cu films on Si substrate using the same technique. Their results showed that the yield stress of Cu films is well described by the dimensional constraint model proposed by Nix[2] combined with classical Hall-Petch grain-size strengthening or Taylor strain hardening. Spolenak et al.[32] studied electroplated and sputter-deposited Cu films on substrates and found that the yield stress at room temperature increases with decreasing film thickness for both sets of films. The sputtered films, however, exhibited a higher yield stress than the electroplated films. This was attributed to the different microstructure of these films. Yu and Spaepen[18] measured the stress-strain curves of electron beam-evaporated Cu thin films on polyimide substrates using a microtensile tester. They reported a 20% modulus deficit and a strong dependence of the yield strength on film thickness.

Although understanding the mechanical behavior of Cu films on substrates is important because, in many applications, Cu films are indeed bonded to a substrate, it is difficult to separate the film thickness effect from grain-size strengthening in films on substrates. To gain better understanding, it is desirable to investigate the behavior of freestanding films. Work on freestanding Cu films can be traced back to the 1960s.[33–36] For rolled Cu foils with thickness varying from 2–150 μm, the strength was reported to be independent of film thickness.[33,34] Oding and Aleksanyan[35] found that the strength of evaporated films decreased by a factor of two when their thickness increased from 1.5 to 4.6 μm. Leidheiser and Sloope[36] studied the stiffness and fracture strength of freestanding thermally evaporated Cu films with thickness ranging from 60–500 nm using a circular bulge test technique. They found that the fracture strength of these films varied inversely with film thickness, whereas the stiffness was the same as for bulk polycrystalline Cu, independent of film thickness. No correlation of the mechanical properties with the microstructure of the films was made. Recently, Read and colleagues[20,37,38] studied the tensile, fracture, and fatigue behavior of freestanding electron beam-evaporated Cu thin films using the microtensile test. The Cu films exhibited low ductility, which was attributed to a lack of dislocation sources and a dislocation glide distance limited by the film thickness and fine grain size.

In our research, we systematically investigated the mechanical properties and microstructure of freestanding electroplated Cu thin films using the plane-strain bulge test. Specifically, we evaluated the effects of film thickness, grain size, and crystallographic texture on the mechanical behavior of the films.

II. EXPERIMENTAL

Silicon wafers with (100) orientation were coated on both surfaces with 80 nm of Si_3N_4 using low-pressure chemical vapor deposition. Before the Cu plating process, a 20-nm TaN adhesion layer and a thin Cu seed layer were sputter deposited onto the Si_3N_4 coating. Cu films with a thickness ranging from 0.9–3.0 μm were electroplated using a proprietary plating process.[39] Immediately after the electroplating process, the Cu films have a grain size on the order of a few tens of nanometers. As-plated films recrystallize spontaneously at room temperature over a period of a few hours to several days. This is a phenomenon commonly observed for electroplated films.[39–42] In this work, only fully recrystallized films were investigated. These films will be called "as-deposited films." To increase the grain size, half of the films were annealed for 1 h in a vacuum furnace (~10^{-7} Torr) at 600 °C. These films will be referred to as "annealed films." As listed in Table I, six sets of samples were prepared for this study.

The microstructure of the Cu films was characterized using focused ion beam microscopy (FIB) in a Dual-Beam FIB/SEM DB235 system (FEI Company, Hillsboro, OR). Plan-view transmission electron microscope (TEM) samples were prepared and the sub-grain structure of the films was characterized in a transmission

TABLE I. Summary of results.

Film set	Film thickness t (μm)	Mean grain size (μm) Regular grain	Mean grain size (μm) Twin	Fraction of ⟨111⟩ texture	Plane-strain modulus (GPa)	0.2%-σ_y (MPa)
As-deposited[a]	0.9	1.82 ± 0.57	0.41 ± 0.02	58	154 ± 5	294.9 ± 1.3
	1.8	1.91 ± 0.09	0.53 ± 0.01	42	143 ± 4	265.5 ± 1.6
	3.0	1.95 ± 0.37	0.65 ± 0.18	30	135 ± 5	252.3 ± 1.2
Annealed[b]	0.9	2.99 ± 0.18	0.98 ± 0.14	52	N/A[c]	N/A[c]
	1.8	3.00 ± 0.43	1.34 ± 0.34	40	138 ± 3	161.1 ± 5.3
	3.0	6.13 ± 0.38	2.47 ± 0.3	31	119 ± 6	119.6 ± 4.8

[a]After spontaneous recrystallization at room temperature.
[b]Annealing conditions: 600 °C at 10^{-7} Torr for 1 h.
[c]The annealed 0.9-μm films broke at an early stage during the bulge test.

electron microscope (model 420T; Philips, Mahwah, NJ) before and after deformation. The crystallographic texture of the films was determined with x-ray diffraction (XRD) in a D5000 diffractometer (Siemens, New York, NY).[39] The surface topology was analyzed using scanning electron microscopy (SEM) in a DualBeam system (FEI Company) and with atomic force microscopy (AFM) in a Nanoscope IIIA Multimode STM (Digital Instruments, Santa Barbara, CA).

The stress-strain curves of these films were measured by means of the plane-strain bulge test. In this test, long rectangular membranes are fabricated out of the material of interest and deformed through application of pressure as illustrated schematically in Fig. 1. A detailed description of the technique and the sample preparation process has been published elsewhere.[27,28,43] Briefly, after deposition of the Cu film, a layer of benzocyclobutene is spin coated to protect the Cu film during sample preparation. Photolithography is used to define long rectangular windows in the Si_3N_4 coating on the backside of the Si substrate. The exposed Si substrate is etched anisotropically using a potassium hydroxide based solution with the Si_3N_4 on the front side of the substrate serving as etch stop. Freestanding Cu membranes are obtained by removing the Si_3N_4/TaN layer using a reactive ion etch with CF_4 and by dissolving the benzocyclobutene protective coating in a proprietary solvent supplied by Dow Chemical (Midland, MI). During a bulge test experiment, a Cu film is deformed by applying a uniform pressure to one side of the Cu membrane (Fig. 1). The pressure, p, is measured with a pressure sensor and the corresponding membrane deflection, h, with a He-Ne laser interferometer. The stress and strain in the membrane are determined independently from the pressure and deflection using the following analytical formulae[27,43]

$$\sigma = \frac{p(a^2 + h^2)}{2ht} \quad \text{and}$$

$$\epsilon = \epsilon_0 + \frac{a^2 + h^2}{2ah} \arcsin\left(\frac{2ah}{a^2 + h^2}\right) - 1 \quad , \qquad (1)$$

where t is the film thickness, $2a$ is the width of the membrane, as shown in Fig. 1(a), and ϵ_0 is the equi-biaxial residual strain in the film. The Cu films were tested in an essentially quasistatic process with a nominal constant strain rate of 1.3×10^{-6} s^{-1}. Partial unloading cycles were imposed to extract the elastic properties of the films. All films were loaded until final rupture.

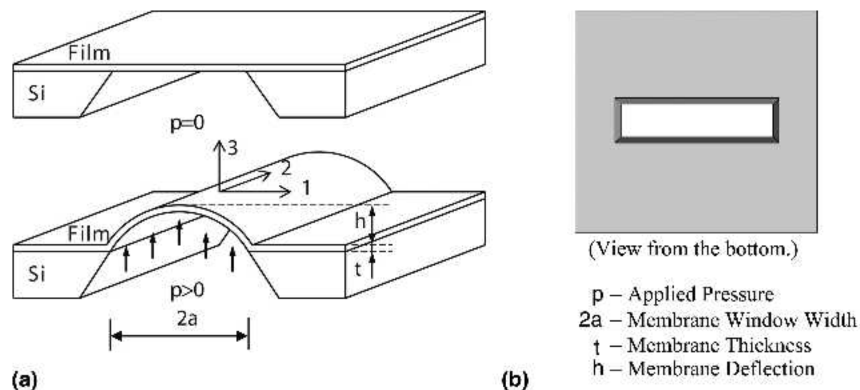

FIG. 1. Schematic of the plane-strain bulge test technique for thin films. (a) Perspective view of a freestanding membrane before and after pressure is applied; (b) plan view of the sample showing a long rectangular window in a Si substrate.

III. RESULTS

A. Microstructural characterization

Table I summarizes key microstructural information for the Cu films in this study. The grain structure of as-deposited and annealed films is shown in the FIB micrographs in Fig. 2. As is evident from the micrographs in Figs. 2(a)–2(c), as-deposited films have a very high incidence of twinning. The films show evidence of abnormal grain growth, and a few <100> grains as large as 6–8 μm are observed. If only regular grain boundaries are counted, the average grain size is approximately 1.9 μm in all as-deposited films, independent of film thickness. However, if twin boundaries are counted as grain boundaries, the average grain size is much smaller and scales with film thickness. The average grain sizes obtained using both approaches are tabulated in Table I. After annealing at 600 °C for 1 h, normal grain growth is observed in all films [Figs. 2(d)–2(f)]. The average grain size of the annealed films increases significantly with film thickness (Table I); abnormal grains grow only slightly to a size of approximately 8–9 μm.

The orientation distribution functions (ODF) of the films were calculated from the XRD data[39] following the methodology described in Ref. 44. They are presented in Fig. 3 for as-deposited and annealed films. The as-deposited films generally have textures with distinct <111>, <100>, and <110> fiber components in addition to a significant fraction of randomly oriented grains. The texture of the thinnest films is dominated by a sharp <111> fiber component, but this component decreases with increasing film thickness, and the random texture component increases. The volume fraction of the <111> component calculated from the ODFs is listed as a function of film thickness in Table I. Annealing does not produce significant changes in the texture. Only a slight weakening of the <111> texture in the thinner films was observed (Table I).

The plan-view TEM images in Fig. 4 reveal the microstructure of some of the films before and after deformation. The micrographs in Figs. 4(a) and 4(b) are for an as-deposited 1.8-μm film before deformation. The film is polycrystalline with many growth twins [Fig. 4(a)], confirming the FIB results. At higher magnification [Fig. 4(b)], areas with much smaller grains can be observed. Presumably, these areas did not fully recrystallize after the electroplating process. It should be noted that this morphology is distinctly different from the porous sub-grain structure composed of agglomerated spheroids observed by Read et al.[20] in Cu electrodeposits. Figure 4(c) shows a micrograph of a 1.8-μm film after annealing. The heat treatment results in a significant increase in grain size. In some grains, a high density of slip traces is observed [Fig. 4(c)]. These slip traces form in the annealed films because of the thermal mismatch between film and substrate when the samples are cooled down after annealing. Annealed films are subjected to a strain of approximately 0.7% during cooling and, consequently, they have a relatively high dislocation density. Figure 4(d) shows a typical micrograph for an annealed 3.0-μm film after deformation to approximately 3% of plastic strain. High dislocation densities are visible in most grains of the deformed film.

Although as-deposited films have a smooth surface, annealed films show significant topography near the grain boundaries. Figure 5 presents AFM results for the

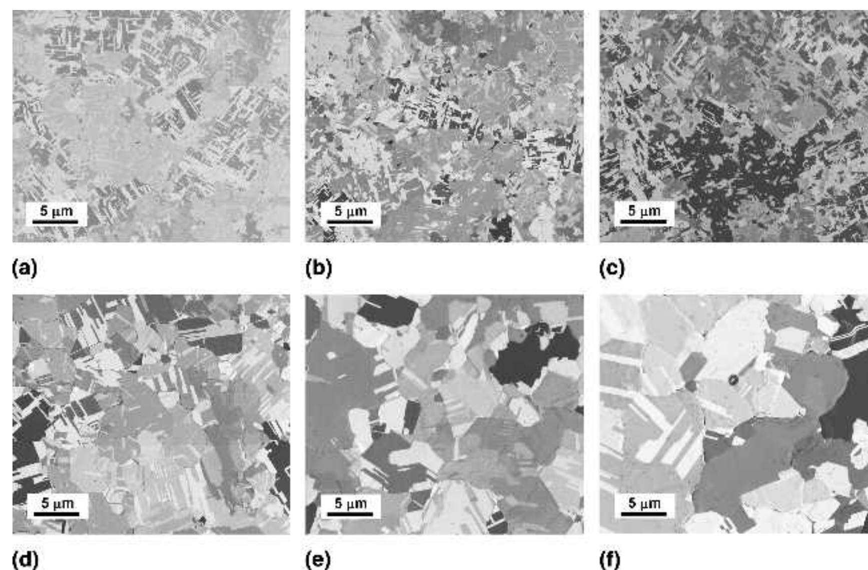

FIG. 2. FIB micrographs showing the grain structure of as-deposited [(a), (b), and (c) for t = 0.9, 1.8, and 3.0 μm, respectively] and annealed [(d), (e), and (f) for t = 0.9, 1.8, and 3.0 μm, respectively] Cu films.

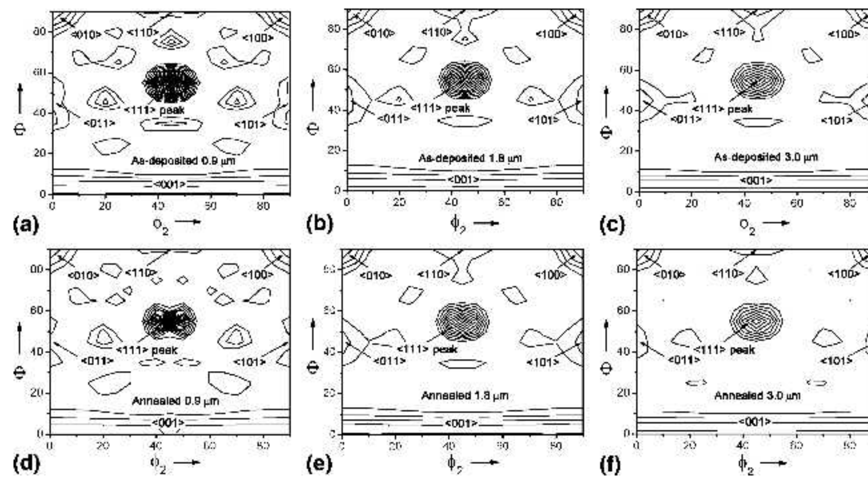

FIG. 3. The ODF of as-deposited [(a), (b), and (c) for t = 0.9, 1.8, and 3.0 μm, respectively] and annealed [(d), (e), and (f) for t = 0.9, 1.8, and 3.0 μm, respectively] Cu films as a function of the three Euler angles.

surface morphology of annealed 1.8-μm [Figs. 5(a) and 5(b)] and 3.0-μm [Figs. 5(c) and 5(d)] films. A significant degree of grooving and hillocking is observed along high-angle grain boundaries in both films [Figs. 5(a) and 5(c)]. Thicker films have deeper and better-defined grain boundary grooves than thinner films. Cross-sectional depth profiles are shown in Figs. 5(b) and 5(d). Deep grooves along the grain boundary are often accompanied with hillocks on either side of the grain boundary, suggesting a mass flux from the grain boundaries to the film surface during the annealing process.[45] The average depth of the grooves is approximately 40 nm for the 1.8-μm film and 190 nm for the 3.0-μm film. Similar observations on grain boundary morphological changes in annealed Cu films have been reported by Joo et al.[46]

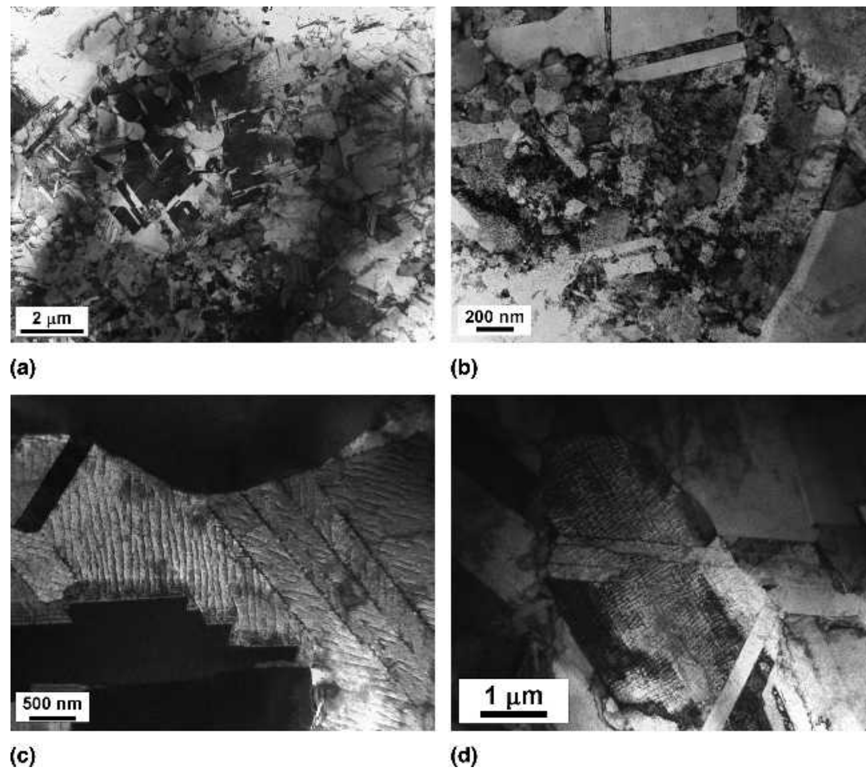

FIG. 4. TEM micrographs showing the grain structure of a 1.8-μm untested Cu film, (a, b) before, (c) after annealing, and (d) a 3.0-μm annealed Cu film after deformation in the bulge test.

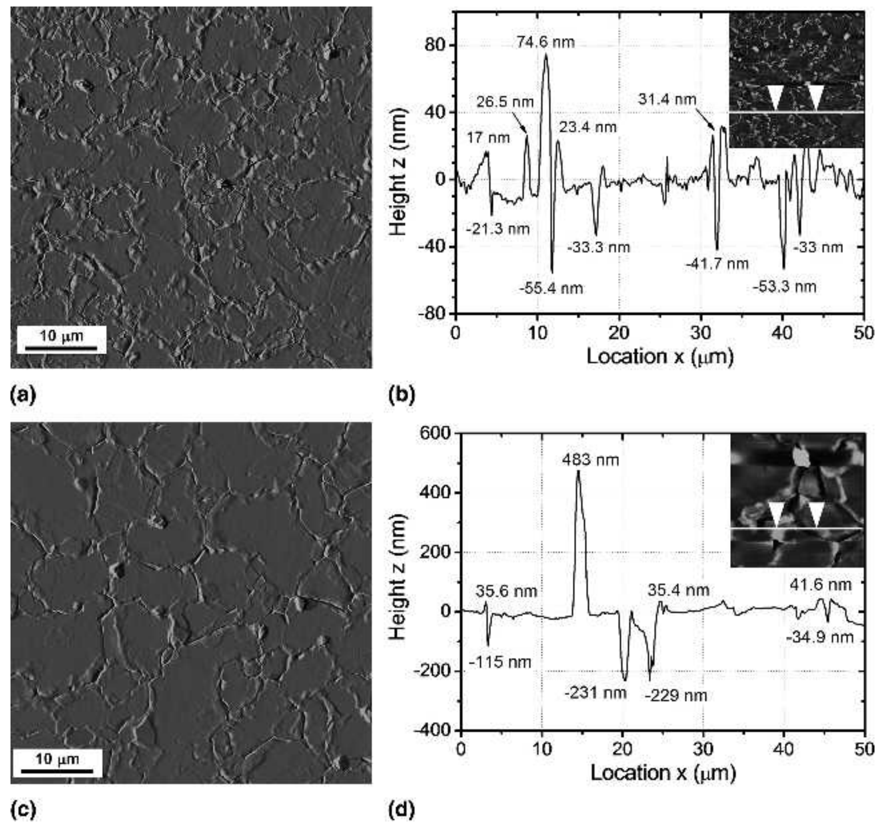

FIG. 5. AFM results showing grain boundary morphology of annealed (a, b) 1.8-μm and (c, d) 3.0 μm Cu films. (a, c) Plan view in deflection mode; (c, d) cross-sectional profile showing the extrusion heights and groove depths.

B. Mechanical properties

Typical stress-strain curves for as-deposited and annealed Cu films are presented in Fig. 6. No data for the annealed 0.9-μm films were obtained because the membranes fractured early in the test. A maximum strain of approximately 4.5% was obtained for the annealed 3.0-μm films (only the first 1.5% is shown in Fig. 6). The residual stress in the films is on the order of 100 MPa before annealing and decreases after the heat treatment. The plane-strain modulus, $M = E/(1 - \nu^2)$, where E is Young's modulus and ν is Poisson's ratio, is obtained from the slopes of the unloading curves and is plotted as a function of the film thickness in Fig. 7 for as-deposited and annealed films. Before annealing, the plane-strain

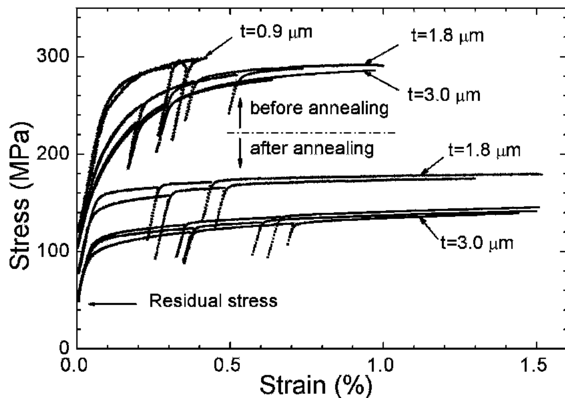

FIG. 6. The plane-strain stress-strain curves of freestanding electroplated Cu films.

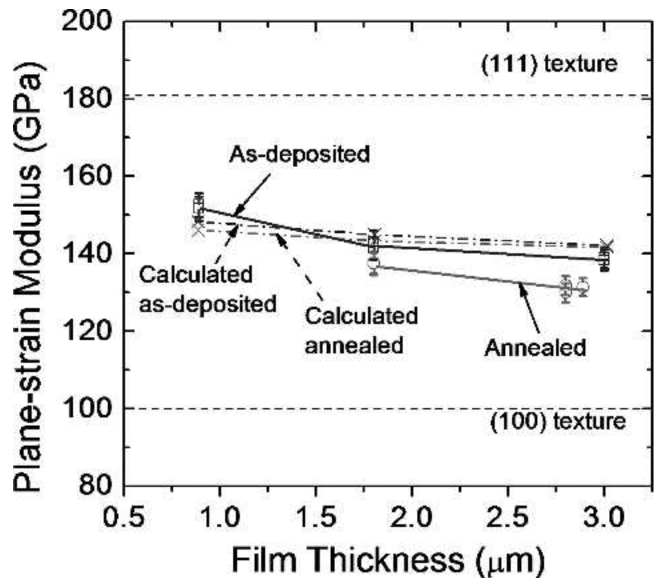

FIG. 7. The variation of stiffness with film thickness and heat treatment.

modulus varies from 138 to 151 GPa with decreasing film thickness. Annealing results in a slight decrease of the stiffness of the films. For reference, the plane-strain modulus of bulk, polycrystalline Cu is approximately 136 GPa.[47] As-deposited, thicker films have a more gradual transition from elastic to plastic behavior compared with thinner films. For the same thickness, annealing leads to a much sharper transition in all films. After the films yield completely, there is no significant difference in the strain-hardening behavior of as-deposited and annealed films. In this study, the plane-strain yield stress, σ_y, is defined at an offset plastic strain of 0.2%. The corresponding values are tabulated in Table I and are plotted as a function of film thickness in Fig. 8(a). The yield stress increases slightly with decreasing film thickness and drops significantly after annealing.

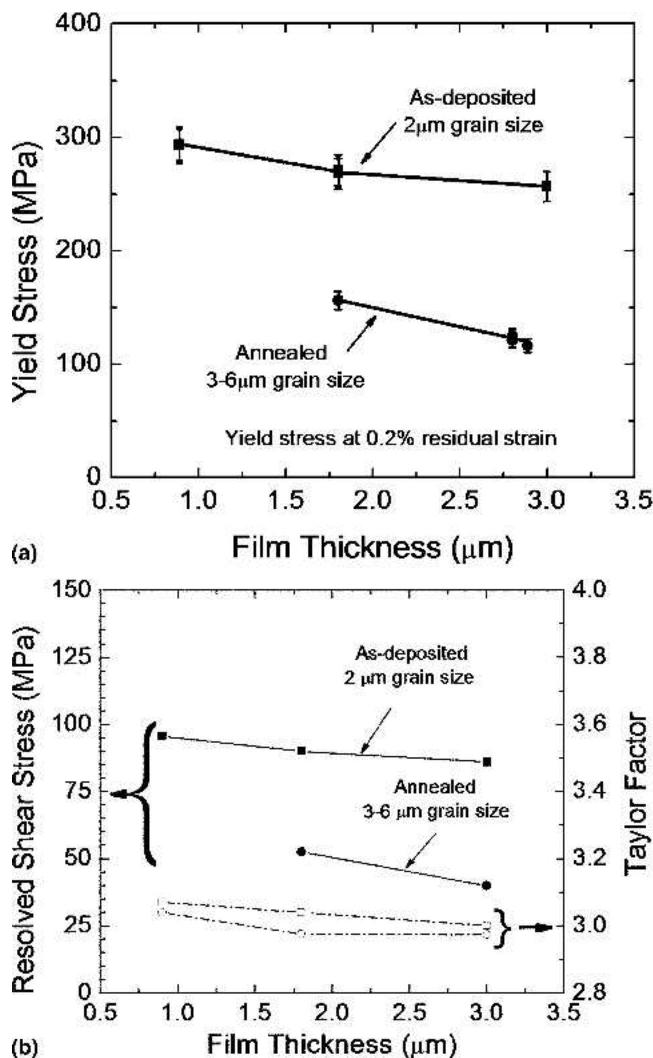

FIG. 8. (a) Plane-strain yield stress as a function of film thickness and heat treatment. (b) Resolved shear stress (solid lines and filled symbols) and the plane-strain Taylor factor (dash-dot lines and open symbols) as a function of film thickness and heat treatment. Squares and circles represent as-deposited and annealed films, respectively.

IV. DISCUSSION

A. Elastic modulus

The stiffness of the Cu films increases with decreasing film thickness for as-deposited and annealed films. This variation is related to the change in crystallographic texture of these films because Cu is an elastically anisotropic material with a stiffness that is strongly orientation dependent. For example, the theoretical plane-stain modulus of Cu films with a pure <111>-, <110>-, and <100>-fiber texture can be calculated from the single-crystal elastic constants of bulk Cu to be 181, 156, and 99 GPa, respectively. With reference to Table I, the <111>-fiber texture component is present in all films, and the volume fraction of this component increases with decreasing film thickness. Thus, one would expect the modulus of the Cu films to increase with the volume fraction of the <111>-texture component. To verify this, the theoretical values of the plane-strain moduli of these samples were calculated based on the experimental orientation distribution functions (see Fig. 3) using the single-crystal elastic constants of Cu.[48] The detailed analysis is given in Appendix A and the results are presented in Fig. 7, together with the experimental data. For comparison, the theoretical plane-strain moduli of films with pure <111>- and <100>-fiber textures, which constitute the theoretical upper and lower bounds for the plane-strain modulus, are also shown in Fig 7.

For the as-deposited films, agreement between experimental and calculated values is quite remarkable. After annealing, the plane-strain modulus decreases slightly. This decrease cannot be attributed to the crystallographic texture because the texture of these films remains nearly unchanged after annealing. One possible explanation for the reduced modulus is the severe grain boundary grooving observed after annealing (Fig. 5). The effect of grain boundary grooving on the film stiffness can be estimated by modeling the grooves as a periodic array of cracks. The reduction in film stiffness caused by the cracks is readily determined from a fracture mechanics analysis[49] and is, at most, 1%–2%, too small to explain the decrease in stiffness upon annealing. A more likely explanation may be found in enhanced anelastic behavior of the annealed films. This explanation is indeed supported by experimental results obtained by Kalkman and colleagues,[19] who used a dynamic bulge test technique to demonstrate that the stiffness of freestanding Cu films is frequency dependent. They attributed this observation to anelastic stress relaxation resulting from grain boundary sliding. Dislocation bowing is a more likely mechanism in the present case because the annealed films have larger grains than the as-deposited films and they have high dislocation densities [Figs. 4(c) and 4(d)].

In our experiments, no modulus deficit was found. This is consistent with measurements by Espinosa et al.[22]

on freestanding, sputter-deposited Cu film using a membrane deflection technique. Spaepen and colleagues[17,18] reported an approximately 20% reduction in modulus for electron beam-evaporated Cu films using a microtensile test. They attributed this reduction to incomplete cohesion ("microcracking") of the grain boundaries during the vapor deposition process. Read et al.[20] reported an even higher (30%–50%) modulus deficit in electroplated Cu films. In this case, the reduced stiffness was attributed to film porosity and plating defects. Based on these studies, it seems that the modulus deficit is more related to the film deposition technique and the ensuing microstructure rather than an intrinsic thin film effect.

B. Stress-strain curves and residual stresses

Before annealing, the stress-strain curves exhibit a gradual transition from elastic to plastic deformation. This gradual transition can be attributed to variations in the residual stress between grains. It is indeed well known from microdiffraction experiments that the residual stress state can differ significantly from grain to grain.[50] Furthermore, as-deposited films have a heterogeneous microstructure with large grains next to areas of smaller grains and thus higher yield stress. Consequently, different grains yield at different overall stress levels producing a rounded stress-strain curve. Thicker films have a wider grain size distribution, making the transition more gradual for these films.

Annealed films, by contrast, have a sharp elastic-plastic transition. This is explained as follows. After a Cu film is annealed at 600 °C for 1 h, the stress in the film is more or less fully relaxed because of diffusional processes. When the film is cooled to room temperature, a tensile stress develops in all grains because of the thermal mismatch between film and substrate. Considering the magnitude of the thermal mismatch strain, full plastic flow is expected in all grains. Thus, immediately after cooling, all grains are roughly at their yield stress. This stress is relaxed somewhat during the wet etch process as is evident from the stress-strain curves in Fig. 6. Consequently, all grains are expected to yield at almost the same macroscopic strain with some variation from grain to grain resulting from the stress relaxation and the elastic anisotropy of the grains. Macroscopically, this results in a sharp transition of the stress-strain curve from the elastic regime to the plastic regime. It should be noted that the elastic-plastic transition also depends on the crystallographic texture of the films because some grains are oriented more favorably for plastic deformation than others. The effect of texture is not important in this case, however, because as-deposited films and annealed films of a given thickness have similar textures (see ODFs in Fig. 3) and yet sharply different transitions. This indicates that the gradual transition for the as-deposited films can be attributed mainly to grain-to-grain variations in the residual stress and to the heterogeneity of the microstructure.

C. Yield stress

Figure 8(a) shows the yield stress of the Cu films as a function of film thickness. The figure clearly illustrates that the film thickness is not the main parameter determining the yield stress of the films. Potential strengthening mechanisms in these Cu films include grain boundary strengthening, Taylor hardening, the film thickness effect, the effect of crystallographic texture, and, possibly, solid solution hardening by impurities that were introduced in the films during the electroplating process. Strengthening from the film thickness effect can be ruled out in the present study because the films in this study are freestanding and Cu does not form a strong passivating oxide layer. In fact, one might even expect a slight weakening of a freestanding film when the film thickness is on the order of the grain size because of a reduction in constraint experienced by each grain. Strengthening from dislocation interactions is also unlikely to be a significant factor because the increase in flow stress from work hardening in Fig. 6 is small compared with the reduction in yield stress after annealing. Moreover, the annealed films have a relatively high dislocation density. Finally, it is likely that electroplated Cu films have small amount of impurities from the electroplating process, but the concentration of impurities and the resulting solid solution strengthening should be independent of film thickness or heat treatment. Thus, crystallographic texture and grain size are the main candidates in explaining the observed behavior. These strengthening mechanisms will now be examined in more detail.

The yield stress of polycrystalline films depends on the texture of the films because grains with different orientations yield at different levels of stress. To quantify this effect, the plane-strain Taylor factor was calculated from the experimental ODFs for each of the films. Details of the calculation can be found in Appendix B. Figure 8(b) shows the Taylor factor and the corresponding resolved shear stress as a function of film thickness. The Taylor factor decreases slightly with increasing film thickness and after annealing, but the effect is not nearly strong enough to explain the experimental observations: the resolved shear stress varies with film thickness and with heat treatment.

We now consider the effect of grain boundary strengthening. Figure 9(a) shows the plane-strain yield stress of the films in a traditional Hall-Petch plot. The correlation with the square root of the grain size is poor, with different slopes for annealed and as-deposited films. In Fig. 9(b), the yield stress is plotted as a function of the modified average grain size, counting twin boundaries as distinct grain boundaries. The yield stress clearly shows Hall-Petch behavior, indicating that twin boundaries act

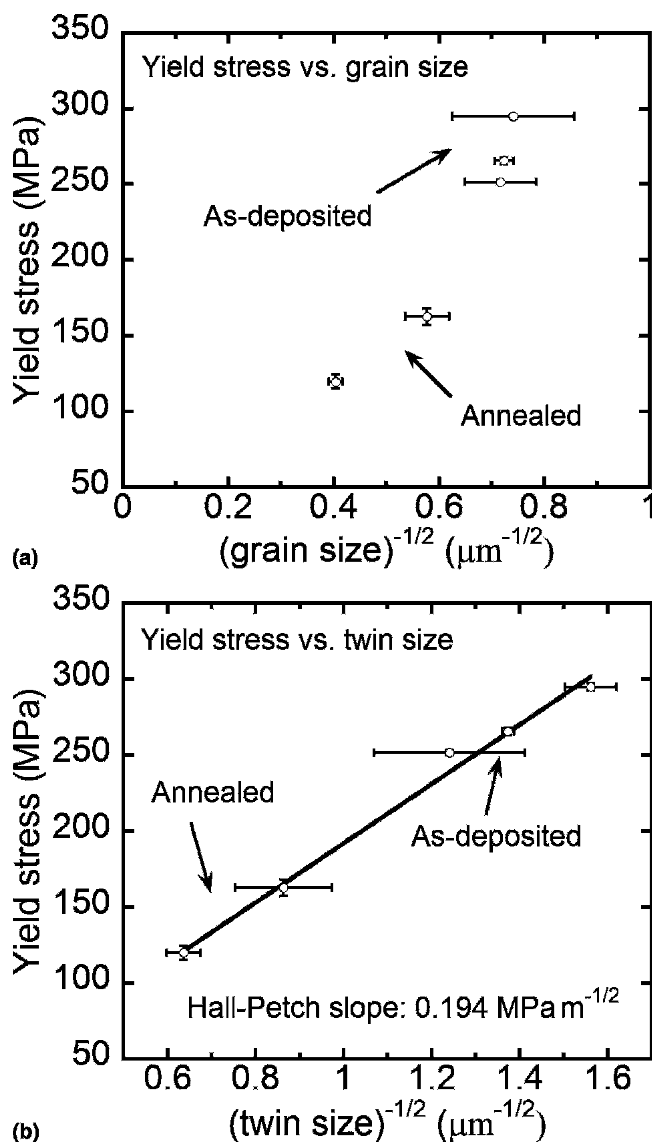

FIG. 9. The plane-strain yield stress as a function of average grain size, (a) ignoring twin boundaries and (b) taking twin boundaries into account.

as barriers to dislocation motion. Dislocations with Burgers vectors along the intersection of the slip planes in the twinned and untwinned sections of the grain can of course propagate across the twin boundary. Transmission of dislocations with other Burgers vectors, however, requires these dislocations to first dissociate into a nonglissile Frank partial dislocation that is left at the twin boundary and a Shockley partial dislocation that can propagate through the boundary. The dissociation process is energetically unfavorable and requires an elevated stress level before it occurs.[51] This mechanism is confirmed by a TEM study of bulk electroplated Cu samples with very high twin densities[51] and by in situ TEM observations of the deformation process in nanocrystalline Cu specimens.[52] Thus, twin boundaries can be treated as obstacles to dislocation motion, and our results suggest that the relevant length scale in the Hall-Petch relationship is the modified average grain size where twins are counted as separate grains. It should be noted that the difference between the two measures for grain size, and hence the difference between Figs. 9(a) and 9(b), is a direct consequence of the high incidence of twinning in these films and may not be so obvious for films with fewer twins. The data in Fig. 9(b) suggest a Hall-Petch coefficient of 0.194 ± 0.011 MNm$^{-3/2}$. However, to make a valid comparison with the bulk Hall-Petch coefficient for Cu, the results in Fig. 9(b) first need to be converted to the equivalent uniaxial yield stress using the procedure discussed in Ref. 27. The resulting Hall-Petch slope is 0.156 ± 0.008 MNm$^{-3/2}$, which is in good agreement with the value of 0.112 MNm$^{-3/2}$ observed in tensile testing of bulk Cu.[53] It should be noted that the grain sizes used to determine the Hall-Petch coefficient for these samples are slightly larger than for equivalent bulk samples with more equiaxed grains because of the large aspect ratios of twins. Properly correcting for the aspect ratios of the twins further lowers the Hall-Petch coefficient to the bulk value.

Keller et al.[31] obtained a Hall-Petch coefficient roughly three times larger than that of bulk Cu by testing sputter-deposited Cu films on Si substrates using the substrate curvature technique. Interpretation of substrate curvature measurements is complicated by the fact that temperature and strain are changed simultaneously during the measurement. Furthermore, it is difficult to separate the effects of grain size and film thickness for films on substrates. This clearly illustrates the importance of making measurements on freestanding films.

V. CONCLUSIONS

In this study, the plane-strain bulge test technique was used to investigate the mechanical behavior of freestanding electroplated Cu thin films with an eye on the effects of film thickness and microstructure. A small variation of stiffness with Cu thickness was observed. This variation is the result of the elastic anisotropy of Cu and the changes in the crystallographic texture of the films. The Cu films do not show a modulus deficit, and experimental moduli agree well with results obtained from single-crystal elastic constants and the appropriate orientation distribution functions. Variations of yield stress with film thickness and heat treatment can be directly attributed to corresponding changes in the grain size of the films. The measurements indicate that twin boundaries act as obstacles to dislocation motion, and the yield stress follows typical Hall-Petch behavior if twins are counted as distinct grains when determining the grain size. Film thickness and crystallographic texture have a negligible effect on strengthening of freestanding Cu thin films.

ACKNOWLEDGMENTS

We thank M.T. Perez-Prado for assistance with XRD, W. MoberlyChan for help with the TEM work, and Y-S. Jun for use of the AFM. Helpful discussions with J.W. Hutchinson and F. Spaepen are gratefully acknowledged. This research was funded by the National Science Foundation (Grant No. DMR-0133559) and by the MRSEC at Harvard University.

REFERENCES

1. R.P. Vinci and J.J. Vlassak: Mechanical behavior of thin films. *Annu. Rev. Mater. Sci.* **26,** 431 (1996).
2. W.D. Nix: Mechanical properties of thin films. *Metall. Trans. A* **20,** 2217 (1989).
3. E. Arzt: Size effects in materials due to microstructural and dimensional constraints: A comparative review. *Acta Mater.* **46,** 5611 (1998).
4. N. Triantafyllidis and E.C. Aifantis: A gradient approach to localization of deformation. 1. Hyperelastic materials. *J. Elast.* **16,** 225 (1986).
5. E.C. Aifantis: Gradient deformation models at nano, micro, and macro scales. *J. Eng. Mater. Technol.* **121,** 189 (1999).
6. N.A. Fleck, G.M. Muller, M.F. Ashby, and J.W. Hutchinson: Strain gradient plasticity: Theory and experiment. *Acta Metall.* **42,** 475 (1994).
7. N.A. Fleck and J.W. Hutchinson: A reformulation of strain gradient plasticity. *J. Mech. Phys. Solids* **49,** 2245 (2001).
8. N.A. Fleck and J.W. Hutchinson: Strain gradient plasticity. *Adv. Appl. Mech.* **33,** 295 (1997).
9. N.A. Fleck and J.W. Hutchinson: A phenomenological theory for strain gradient effects in plasticity. *J. Mech. Phys. Solids* **41,** 1825 (1993).
10. L. Nicola, E. Van der Giessen, and A. Needleman: Discrete dislocation analysis of size effects in thin films. *J. Appl. Phys.* **93,** 5920 (2003).
11. A. Needleman and E. Van der Giessen: Discrete dislocation and continuum descriptions of plastic flow. *Mater. Sci. Eng. A* **309,** 1 (2001).
12. G.E. Dieter: *Mechanical Metallurgy*, 3rd ed. (McGraw-Hill, New York, 1986), p. 287.
13. F. Spaepen and D.Y.W. Yu: A comparison of the strength of multilayers, thin films and nanocrystalline compacts. *Scripta Mater.* **50,** 729 (2004).
14. M.A. Haque and M.T.A. Saif: Mechanical behavior of 30-50 mn thick aluminum films under uniaxial tension. *Scripta Mater.* **47,** 863 (2002).
15. J. Schiotz, F.D. Di Tolla, and K.W. Jacobsen: Softening of nanocrystalline metals at very small grain sizes. *Nature* **391,** 561 (1998).
16. Z.W. Shan, E.A. Stach, J.M.K. Wiezorek, J.A. Knapp, D.M. Follstaedt, and S.X. Mao: Grain boundary-mediated plasticity in nanocrystalline nickel. *Science* **305,** 654 (2004).
17. H.B. Huang and F. Spaepen: Tensile testing of free-standing Cu, Ag and Al thin films and Ag/Cu multilayers. *Acta Mater.* **48,** 3261 (2000).
18. D.Y.W. Yu and F. Spaepen: The yield strength of thin copper films on Kapton. *J. Appl. Phys.* **95,** 2991 (2004).
19. A.J. Kalkman, A.H. Verbruggen, and G.C.A.M. Janssen: Young's modulus measurements and grain boundary sliding in freestanding thin metal films. *Appl. Phys. Lett.* **78,** 2673 (2001).
20. D.T. Read, Y.W. Cheng, and R. Geiss: Morphology, microstructure, and mechanical properties of a copper electrodeposit. *Microelectron Eng.* **75,** 63 (2004).
21. D.T. Read, Y.W. Cheng, R.R. Keller, and J.D. McColskey: Tensile properties of free-standing aluminum thin films. *Scripta Mater.* **45,** 583 (2001).
22. H.D. Espinosa, B.C. Prorok, and B. Peng: Plasticity size effects in free-standing submicron polycrystalline FCC films subjected to pure tension. *J. Mech. Phys. Solids* **52,** 667 (2004).
23. M.A. Haque and M.T.A. Saif: Deformation mechanisms in free-standing nanoscale thin films: A quantitative in situ transmission electron microscope study. *Proc. Natl. Acad. Sci. USA* **101,** 6335 (2004).
24. Y. Xiang, X. Chen, and J.J. Vlassak: The mechanical properties of electroplated Cu thin films measured by means of the bulge test technique, in *Thin Films: Stresses and Mechanical Properties IX,* edited by C.S. Ozkan, L.B. Freund, R.C. Cammarata, and H. Gao (Mater. Res. Soc. Symp. Proc. **695,** Warrendale, PA, 2002), p. 189.
25. Y. Xiang, J.J. Vlassak, M.T. Perez-Prado, T.Y. Tsui, and A.J. McKerrow: The effects of passivation layer and film thickness on the mechanical behavior of freestanding electroplated Cu thin films with constant microstructure, in *Thin Films—Stresses and Mechanical Properties X,* edited by S.G. Corcoran, Y-C. Joo, N.R. Moody, and Z. Suo (Mater. Res. Soc. Symp. Proc. **795,** Warrendale, PA, 2004), p. 417.
26. H.J. Lee, G. Cornella, and J.C. Bravman: Stress relaxation of free-standing aluminum beams for microelectromechanical systems applications. *Appl. Phys. Lett.* **76,** 3415 (2000).
27. Y. Xiang, X. Chen, and J.J. Vlassak: Plane-strain bulge test for thin films. *J. Mater. Res.* **20,** 2360 (2005).
28. Y. Xiang and J.J. Vlassak: Bauschinger effect in thin metal films. *Scripta Mater.* **53,** 177 (2005).
29. P.A. Flinn: Measurement and interpretation of stress in copper-films as a function of thermal history. *J. Mater. Res.* **6,** 1498 (1991).
30. M.D. Thouless, J. Gupta, and J.M.E. Harper: Stress development and relaxation in copper-films during thermal cycling. *J. Mater. Res.* **8,** 1845 (1993).
31. R. Keller, S.P. Baker, and E. Arzt: Quantitative analysis of strengthening mechanisms in thin Cu films: Effects of film thickness, grain size, and passivation. *J. Mater. Res.* **13,** 1307 (1998).
32. R. Spolenak, C.A. Volkert, K. Takahashi, S. Fiorillo, J. Miner, and W.L. Brown: Mechanical properties of electroplated copper thin films, in *Thin Films—Stresses and Mechanical Properties VIII,* edited by R. Vinci, O. Kraft, N. Moody, P. Besser, and E. Shaffer, II (Mater. Res. Soc. Symp. Proc. **594,** Warrendale, PA, 2000), p. 63.
33. L.S. Palatnik and A.I. Llinskii: The strength of vacuum condensates of copper. *Sov. Phys. Solid State* **3,** 2053 (1962).
34. A. Lawley and S. Schuster: Tensile behavior of copper foils prepared from rolled material. *Trans. Metall. Soc. AIME* **230,** 27 (1964).
35. I.A. Oding and I.T. Aleksanyan: Mechanical properties of copper films. *Sov. Phys. Dokl.* **8,** 818 (1964).
36. H. Leidheiser and B.W. Sloope: Mechanical properties of copper films. *J. Appl. Phys.* **41,** 402 (1970).
37. R.R. Keller, J.M. Phelps, and D.T. Read: Tensile and fracture behavior of free-standing copper films. *Mater. Sci. Eng. A* **214,** 42 (1996).
38. D.T. Read: Tension-tension fatigue of copper thin films. *Int. J. Fatigue* **20,** 203 (1998).
39. M.T. Perez-Prado and J.J. Vlassak: Microstructural evolution in electroplated Cu thin films. *Scripta Mater.* **47,** 817 (2002).
40. A. Gangulee: Structure of electroplated and vapor-deposited copper films. *J. Appl. Phys.* **43,** 867 (1972).
41. I.V. Tomov, D.S. Stoychev, and I.B. Vitanova: Recovery and recrystallization of electrodeposited bright copper coatings at room temperature. 2. X-ray investigation of primary recrystallization. *J. Appl. Electrochem.* **15,** 887 (1985).
42. H. Lee, W.D. Nix, and S.S. Wong: Studies of the driving force for room temperature microstructure evolution in electroplated copper films. *J. Vac. Sci. Technol. B* **22,** 2369 (2004).
43. J.J. Vlassak and W.D. Nix: A new bulge test technique for the

determination of Young's modulus and Poisson's ratio of thin films. *J. Mater. Res.* **7,** 3242 (1992).
44. S.H. Hong, K.H. Chung, and C.H. Lee: Effects of hot extrusion parameters on the tensile properties and microstructures of SiC_w-2124Al composites. *Mater. Sci. Eng. A* **206,** 225 (1996).
45. H. Gao, L. Zhang, W.D. Nix, C.V. Thompson, and E. Arzt: Crack-like grain-boundary diffusion wedges in thin metal films. *Acta Mater.* **47,** 2865 (1999).
46. Y.C. Joo, S.J. Hwang, and H. Park: The effect of grain boundary characteristics on microstructure and stress void evolution in electroplated and sputtered cu films. *Mater. Sci. Forum* **426-432,** 3481 (2003).
47. C.R. Barrett, W.D. Nix, and A.S. Tetelman: *The Principles of Engineering Materials* (Prentice-Hall, Englewood Cliffs, NJ, 1973).
48. G. Simmons and H. Wang: *Single Crystal Elastic Constants and Calculated Aggregate Properties: A Handbook*, 2nd ed. (MIT Press, Cambridge, MA, 1970).
49. H. Tada, P.C. Paris, and G.R. Irwin: *The Stress Analysis of Cracks Handbook* (Del Research Corporation, Hellertown, PA, 1973).
50. M.A. Phillips, R. Spolenak, N. Tamura, W.L. Brown, A.A. MacDowell, R.S. Celestre, H.A. Padmore, B.W. Batterman, E. Arzt, and J.R. Patel: X-ray microdiffraction: Local stress distributions in polycrystalline and epitaxial thin films. *Microelectron. Eng.* **75,** 117 (2004).
51. L. Lu, Y.F. Shen, X.H. Chen, L.H. Qian, and K. Lu: Ultrahigh strength and high electrical conductivity in copper. *Science* **304,** 422 (2004).
52. C.J. Youngdahl, J.R. Weertman, R.C. Hugo, and H.H. Kung: Deformation behavior in nanocrystalline copper. *Scripta Mater.* **44,** 1475 (2001).
53. R. Armstrong, I. Codd, R.M. Douthwaite, and N.J. Petch: Plastic deformation of polycrystalline aggregates. *Philos. Mag.* **7,** 45 (1962).
54. H-J. Bunge: *Texture Analysis in Materials Science: Mathematical Methods* (Butterworths, London, 1982).
55. U.F. Kocks: Relation between polycrystal deformation and single-crystal deformation. *Metall. Trans.* **1,** 1121 (1970).

APPENDIX A: CALCULATION OF THE PLANE-STRAIN MODULUS OF A POLYCRYSTALLINE FILM

In this section, we detail how the plane-strain modulus of a polycrystalline thin film can be estimated from the single-crystal elastic constants and the experimental orientation distribution function of the film. The following derivation applies to single crystals with cubic symmetry, but it is readily generalized to other crystal symmetries. The crystallographic texture of the polycrystalline film is represented by the orientation distribution function, $f(g)$, defined as the probability density of grains with orientations ranging from g to $g + dg$[54]

$$f(g)\mathrm{d}g = \frac{\mathrm{d}V}{V} \quad , \tag{A1}$$

where dV is the total volume of grains orientated in the range of g to $g + dg$, and V is the total volume of the sample. The orientation element dg can be expressed in terms of the three Eulerian angles (Φ, φ_1, and φ_2)

$$\mathrm{d}g = \frac{1}{8\pi^2}\sin\Phi \mathrm{d}\Phi \mathrm{d}\varphi_1 \mathrm{d}\varphi_2 \quad . \tag{A2}$$

The elastic behavior of an anisotropic single crystal is described by the generalized Hooke's law

$$\epsilon_{ij} = s_{ijkl}\sigma_{kl} \quad , \tag{A3}$$

$$\sigma_{ij} = c_{ijkl}\epsilon_{kl} \quad , \tag{A4}$$

where s_{ijkd} and c_{ijkd} are, respectively, the compliance and stiffness tensors of the single crystal in a Cartesian coordinate system. For crystals with cubic symmetry, the axes of the coordinate system are usually aligned with the edges of the unit cell of the crystal. The elastic constants in other coordinate systems are readily found using tensor transformations

$$s'_{ijkl} = a_{mi}a_{nj}a_{pk}a_{ql}s_{mnpq} \quad , \tag{A5}$$

$$c'_{ijkl} = a_{mi}a_{nj}a_{pk}a_{ql}c_{mnpq} \quad , \tag{A6}$$

where s'_{ijkl} and c'_{ijkl} are the compliance and stiffness tensors in the new coordinate system. The direction cosines a_{ij} can be written in terms of the Eulerian angles of the crystal coordinate system with respect to the new coordinate system

$$A = \begin{bmatrix} \cos\varphi_1 \cos\varphi_2 - \sin\varphi_1 \sin\varphi_2 \cos\Phi & \sin\varphi_1 \cos\varphi_2 + \cos\varphi_1 \sin\varphi_2 \cos\Phi & \sin\varphi_2 \sin\Phi \\ -\cos\varphi_1 \sin\varphi_2 - \sin\varphi_1 \cos\varphi_2 \cos\Phi & -\sin\varphi_1 \sin\varphi_2 + \cos\varphi_1 \cos\varphi_2 \cos\Phi & \cos\varphi_2 \sin\Phi \\ \sin\varphi_1 \sin\Phi & -\cos\varphi \sin\Phi & \cos\Phi \end{bmatrix} \quad . \tag{A7}$$

To determine the effective elastic constants of a polycrystalline film with ODF given by $f(g)$, the single-crystal constants are first transformed to the macroscopic coordinate system attached to the film and then averaged over the volume of the film

$$\bar{s}_{ijkl} = \oint s'_{ijkl}(\varphi_1, \Phi, \varphi_2)\frac{\mathrm{d}V}{V} = \oint s'_{ijkl}(\varphi_1, \Phi, \varphi_2)f(g)\mathrm{d}g \quad , \tag{A8}$$

$$\bar{c}_{ijkl} = \oint c'_{ijkl}(\varphi_1, \Phi, \varphi_2)\frac{\mathrm{d}V}{V} = \oint c'_{ijkl}(\varphi_1, \Phi, \varphi_2)f(g)\mathrm{d}g \quad . \tag{A9}$$

Note that Eq. (A8) represents the iso-stress or Reuss average of the elastic constants, whereas Eq. (A9) represents the iso-strain or Voigt average.

For films with fiber textures, the averaged tensors reflect the symmetry of the film, i.e., they are transversely isotropic. The plane-strain modulus of a transversely

isotropic coating with elastic constants c_{ijkl} and s_{ijkl} is given by

$$M = c_{1111} - \frac{c_{1133}^2}{c_{3333}} = \left[s_{1111} - \frac{s_{1122}^2}{s_{1111}} \right]^{-1} \quad , \qquad \text{(A10)}$$

where the x_3-axis is perpendicular to the film and the x_2-axis points in the direction of plane strain. The Reuss and Voigt averages of the plane-strain modulus of the polycrystalline film are then, respectively,

$$M^R = \left[\bar{s}_{1111} - \frac{\bar{s}_{1122}^2}{\bar{s}_{1111}} \right]^{-1} \quad , \qquad \text{(A11)}$$

$$M^V = \bar{c}_{1111} - \frac{\bar{c}_{1133}^2}{\bar{c}_{3333}} \quad . \qquad \text{(A12)}$$

The Voigt and Reuss averages represent upper and lower bounds for the plane-strain modulus of the polycrystalline film. The average of the bounds provides a good estimate for the modulus of the film

$$M = (M^V + M^R)/2 \quad . \qquad \text{(A13)}$$

Slightly different averaging schemes are possible, but usually do not result in significantly different moduli. The theoretical moduli shown in Fig. 7 were calculated using the single-crystal elastic constants for Cu obtained from Ref. 48.

APPENDIX B: TAYLOR FACTOR FOR POLYCRYSTALLINE THIN FILMS WITH A GIVEN ODF[55]

To evaluate the effect of the crystallographic texture, the Taylor factor was calculated for each of the electroplated films using the experimental orientation distribution functions. A detailed description of the procedure can be found in Ref. 55; in this article, only the main points are highlighted. The basic hypotheses in the Taylor factor calculation are that elastic strains are small compared with plastic strains and that the strain experienced by each grain is exactly equal to the macroscopically imposed strain. Because the macroscopic strain is in principle arbitrary, each grain needs at least five independent slip systems to satisfy this last requirement. The procedure for calculating the polycrystalline behavior is then relatively straightforward. For a given grain orientation $(\varphi_1, \Phi, \varphi_2)$, all possible combinations of five slip systems are considered that produce the macroscopically imposed strain through

$$\epsilon_{ij}^m = \sum_m \mu_{ij}^{(k)} \gamma^{(k)} \quad , \qquad \text{(A14)}$$

where ϵ_{ij}^m is the macroscopic plastic strain tensor transformed to the crystal coordinate system and $\gamma^{(k)}$ is the shear on slip system k. The coefficients μ_{ij} in Eq. (A14) are defined as follows

$$\mu_{ij} = \frac{1}{2}(m_i n_j + m_j n_i) \qquad \text{(A15)}$$

and are known as the Schmid factors for slip system (m, n) where m is the unit normal to the slip plane and n is the unit vector parallel to the slip direction. For a face-centered cubic material such as Cu, there are 12 slip systems and hence $C_{12}^5 = 792$ combinations of five independent slip systems that satisfy Eq. (A14). Of all these combinations, the active set of five slip systems satisfies Bishop and Hill's principle of minimum plastic dissipation

$$W_p = \sum_k \tau_y^{(k)} |\dot{\gamma}^{(k)}| = \text{minimum} \quad . \qquad \text{(A16)}$$

If the critical resolved shear stress $\tau_y^{(k)}$ is the same on all slip systems, this equation reduces to

$$\sum_k |\dot{\gamma}^{(k)}| = \text{minimum} \quad , \qquad \text{(A17)}$$

i.e., the active set of slip systems is the one that minimizes the algebraic sum of shears on each of the slip systems. Once the active slip systems are known for a grain with a given orientation, it is a simple matter to calculate the stress σ_{ij} tensor required to deform the grain

$$\mu_{ij}^{(k)} \sigma_{ij} = \tau_y \quad , \qquad \text{(A18)}$$

where k runs from 1 to 5. Because only five slip systems are active, the stress state can be determined only to within a hydrostatic component. For some grain orientations, it is possible that several sets of slip systems satisfy the Bishop and Hill criterion. In this case, the stress states associated with each of these sets are averaged. The stress tensor thus obtained depends on the orientation $(\varphi_1, \Phi, \varphi_2)$ of the grain. The stress state for the polycrystalline film is determined by averaging the stress tensor over all possible grain orientations using the orientation distribution function, $f(g)$, as a weight function

$$\bar{\sigma}_{ij} = \oint \sigma_{ij}(\varphi_1, \Phi, \varphi_2) f(g) \mathrm{d}g \quad . \qquad \text{(A19)}$$

The hydrostatic stress component is finally determined from the condition that the surface of the film be stress free. In a uniaxial tension experiment, the Taylor factor is defined as the ratio of the uniaxial stress and the critical resolved shear stress

$$M_T = \frac{\sigma_y^o}{\tau_y} \quad . \qquad \text{(A20)}$$

For a polycrystalline material with a random crystallographic texture subjected to uniaxial tension, the above procedure results in the classical value of $M_T = 3.06$. If a state of plane strain is imposed instead and one takes into account the crystallographic textures (Fig. 3) of the specific samples, one obtains the plane-strain Taylor factors plotted in Fig. 8(b). In these calculations, all numerical integrations over the Euler angles were performed with a step size of $\pi/36$.